Journal of Engineering and Technology for Industrial Applications

ISSN ONLINE: 2447-0228

ITEGAM-JETIA

Manaus, v.11 n.54, p. 181-187. July/August., 2025.
DOI: https://doi.org/10.5935/jetia. v11i54.1730

RESEARCH ARTICLE OPEN ACCESS

ENHANCING CHARGE TRANSFER EFFICIENCY IN CCDS USING SILVACO SIMULATIONS

Dahmane Djendaoui[1], Zoubir Becer[2], Themeur Obeidi[3]

[1]Laboratório de Automação Aplicada e Diagnóstico Industrial (LAADI), Universidade de Djelfa
[2]Departamento de Física, Universidade de El-Oued
[3]Faculdade de Ciência e Tecnologia, Universidade de Djelfa.

[1]https://orcid.org/0000-0003-3749-6591, [2]http://orcid.org/0000-0002-8537-9499, [3]http://orcid.org/0009-0000-7573-9270

E-mail: djendaoui.d@gmail.com, becer.zoubir@gmail.com, t.obeidi@univ-djelfa.dz

ARTICLE INFO

Article History
Received: March 18, 2025
Revised: April 20, 2025
Accepted: June 15, 2025
Published: August 31, 2025

Keywords:
Buried-channel Charge-coupled devices (BCCD),
Charge transfer inefficiency (CTI),
Packet signal,
Numerical simulation. SILVACO.

ABSTRACT

In this paper, we investigated the charge transfer efficiency (CTE) of a radiation-damaged charge-coupled device (CCD) subjected to proton radiation levels typical of particle detection, nuclear imaging, and space-borne experiments. The trapping of charge carriers by bulk states is the primary factor affecting CTE in such damaged CCDs. Our analysis focused on examining the CTE as a function of signal level, radiation dose (trap concentration), and temperature. We employed the SILVACO semiconductor simulation software using a two-dimensional numerical model to simulate the dynamic transfer process in a buried-channel CCD (BCCD) with a three-phase clock pulse driver. The simulation, after setting the appropriate physical models and the suggested deep trap levels in the channel region, demonstrated that the CTE exhibits a nonlinear dependence on the signal level, with the charge transfer inefficiency (CTI) peaking at $7x10^{-6}$ at 135 K and reaching a minimum value of $2x10^{-6}$ around 200 K. The simulation results we obtained closely match the experimental data found in the literature, providing us with a deep understanding of the impact of radiation-induced traps on the dynamic charge transfer processes in charge-coupled devices.

Copyright ©2025 by authors and Galileo Institute of Technology and Education of the Amazon (ITEGAM). This work is licensed under the Creative Commons Attribution International License (CC BY 4.0).

I. INTRODUCTION

Charge-coupled devices (CCDs), invented by George Smith and Willard Boyle at Bell Laboratories in 1969 [1], quickly gained prominence in advanced applications such as astronomical imaging and were subsequently popularized in consumer cameras [2, 3]. CCDs are crucial in various fields such as embedded IoT applications due to their advantages, including low cost, low power consumption, high bit density, and high sensitivity [4]. Despite their advantages, CCDs are susceptible to radiation damage [5], which can be categorized into surface and bulk damage. In the context of charge transfer losses in buried channel devices, bulk traps are of primary concern. These traps create energy levels between the conduction and valence bands, capturing electrons and releasing them back into the conduction band after some time [6, 7].

The operation of a Charge-Coupled Device (CCD) begins when photons strike the sensor, triggering the photoelectric effect, which creates pairs of holes and electrons. These electrical charges accumulate in specific regions formed by an array of metal-oxide-semiconductor (MOS) capacitor structures, which act as microscopic charge packet traps in the form of potential wells. For each individual pixel in the final image, the accumulated charge packet corresponds to the intensity of incoming light at that point [8].

The MOS capacitors are strategically arranged with minimal spacing between them, enabling charge transfer from one capacitor to its neighbor through a controlled overflow mechanism between their potential wells. This transfer process must be highly efficient since each packet of charge needs to move through numerous steps before reaching the output stage. This requirement has become even more critical as modern CCDs now incorporate millions of pixels, necessitating thousands of successive transfers for each charge packet.

A crucial metric for CCD performance is the charge transfer efficiency (CTE), which quantifies how effectively charge moves between adjacent pixels. The CTE is expressed as a decimal fraction, with current high-quality CCDs achieving approximately 0.99999. This can alternatively be described using the charge transfer inefficiency (CTI), which is calculated as 1 minus the CTE value. CTI in buried channel charge-coupled devices (BCCDs) is a critical factor affecting device performance. Studies have shown that BCCDs generally exhibit lower CTI compared to surface-channel CCDs (SCCDs) due to reduced interface traps [9]. Optimizing design parameters, such as p-well inclusion over silicon trench isolation (STI) edges, can further reduce CTI in CMOS based CCDs [10]. Controlling the rising and falling times of clock signals significantly improves CTI in BCCDs but has minimal effect on SCCDs [9].

Particle radiation exposure can also significantly degrade the CTI performance of CCDs. Extensive research has demonstrated that the deterioration in CTI following radiation exposure can be attributed to the formation of electron trap sites within the device structure [8]. While the relationship between trapping mechanisms and radiation effects was recognized in early studies, the expanding role of CCDs in space-based applications has driven substantial contemporary research in this field [11]. Additionally, studies have shown that both operating temperature and charge transfer timing play crucial roles in determining CTI performance [12] and we have been able to demonstrate this utilizing advanced transient two-dimensional device simulation since one-dimensional analysis may overestimate charge handling capacity [13]. A comprehensive understanding of these various factors affecting CTI is essential for multiple purposes: it enables more accurate interpretation of CCD-collected data, allows operators to optimize device settings, and guides manufacturers in developing more radiation-resistant devices.

This study is composed of six sections. In the second section, we presented the methods and the used models including the adopted device structure design, the simulation parameters and the clocking voltages. The third section, details the physical model and its governing equations namely; the Poisson's equation and electron continuity equations along with their numerical solution techniques as well as mobility and recombination models offered by SILVACO Atlas. Section four shows the results of our simulations, namely the trapped charge density from transfer of signal charge as function of time. In Section five, we describe the way in which we did the numerical calculation of CTI based on the simulation output and the trapping theory. In Section six the conclusions are given.

II. METHODS AND MODELS

II.1 DEVICE STRUCTURE

In this study, we use the SILVACO simulation package, particularly the Athena and Atlas programs, to perform two-dimensional simulations of CCDs. The simulated device has dimensions of 28.8 µm in length and 110 µm in depth. The structure of the BCCD is illustrated in Figure 1. It comprises three main parts: an input section, a transfer section, and an output section. The input section includes an input dioxide (ID) and input gate (IG) to generate signal charges, potentially through the photoelectric effect. The transfer section consists of a series of MOS capacitors, with each capacitor representing a transfer gate. In our model, three gates (G1, G2, G3) facilitate signal charge transfer using a three-phase clock pulse driver. The output section includes an output dioxide (OD) and output gate (OG) to discharge the signal charges.

The dielectric thickness in the device is 0.16 µm, composed of two layers: Si_3N_4 0.06 µm and SiO_2 0.10 µm. The lengths of the input and output gates are 4 µm each, with a 0.1 µm gap between the transfer gates, which are also 4 µm long. The doping concentrations and junction depths for various parts of the device are specified, with the pixel size being 12x12 µm^2. The minority carrier lifetime is 10^{-7} seconds.

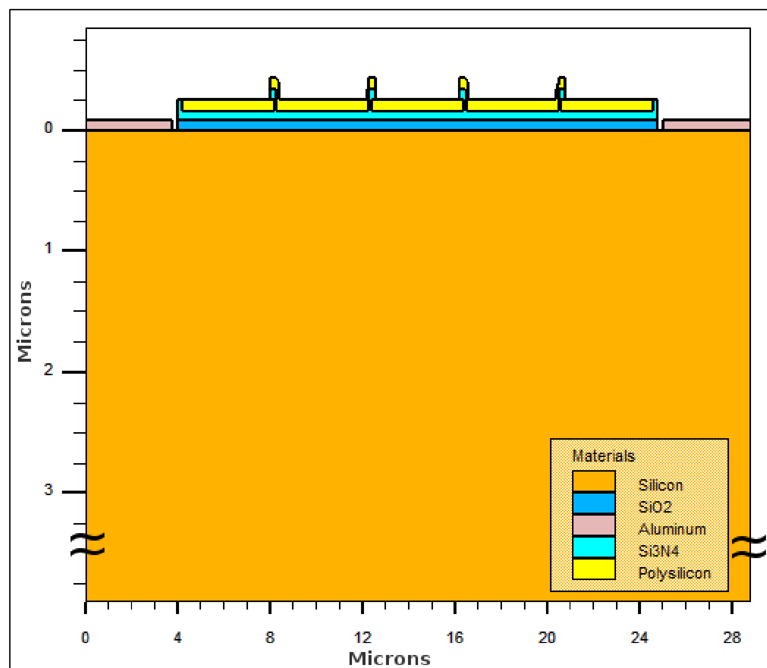

Figure 1: General structure of BCCD (28.8 µm x 110 µm), there are three transfer gates, input part (ID, IG), and output part (OD, OG).
Source: Authors, (2025).

II.2 SIMULATION PARAMETERS

To conduct a successful device simulation, an input file is written in Duckbuild (API interface of SILVACO) to virtually fabricate a BCCD structure using Athina process package, and then pass the built structure to Atlas package for electrical simulation.

Figure 2 shows the mesh of the CCD structure, designed using ATHENA. We refined the mesh size on the buried channel to resolve the doping and charge profiles. The cross-section under gate G2 of the net doping is presented in Figure 3.

During the transfer process, voltages applied to various parts of the device range from -6V to 12V, as detailed in the clock voltage diagram in Figure 4. The CCD circuit is driven by a clock pulse frequency of 4 MHz.

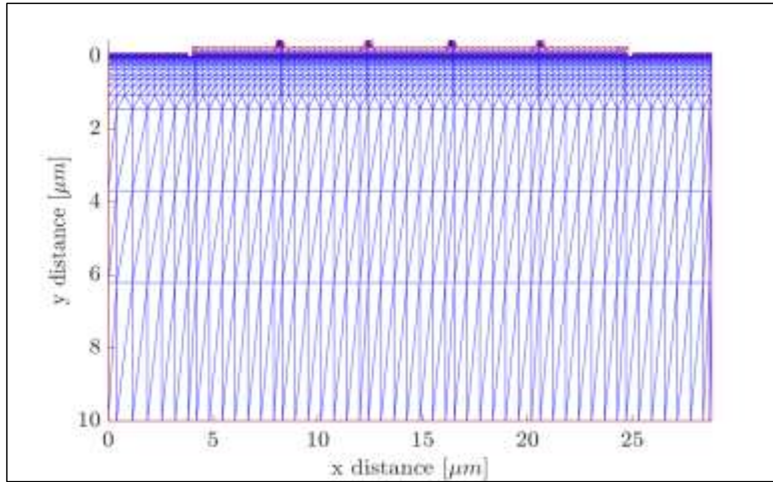

Figure 2: The Mesh use the CCD structure. The mesh size is small on the center of transfer channel.
Source: Authors, (2025).

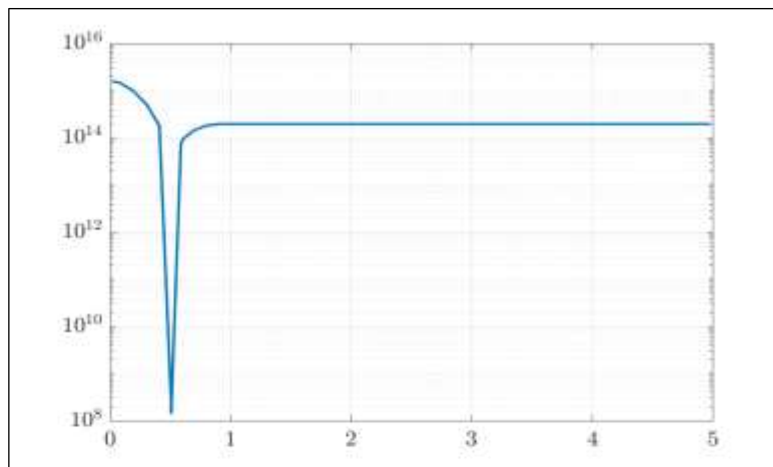

Figure 3: Net doping concentration along the cross-section beneath gate G2.
Source: Authors, (2025).

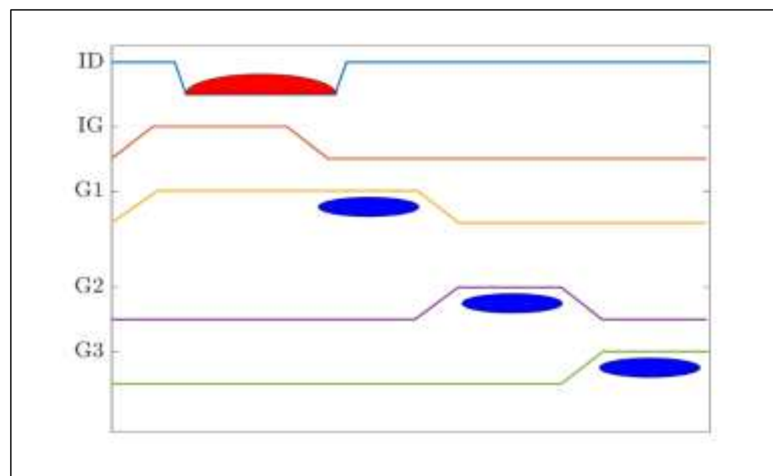

Figure 4: Diagram of clock voltages in a three-phase BCCD. The shaded areas schematically represent the signal charge packet and illustrate how it is transferred by the clock voltages.
Source: Authors, (2025).

III. SIMULATION

III.1 MOBILITY AND RECOMBINATION MODELS

The SILVACO incorporates various mobility and recombination models. Mobility models include concentration mobility, surface mobility, and electric field mobility. Recombination models involve Shockley-Read-Hall (SRH) and Auger recombination processes. The physical models implemented in this simulation represent key physical effects relevant to CCD device performance. The CVT ATLAS mobility model incorporates surface mobility degradation, which plays a critical role during the charge transfer phase, as charge moves from the storage node to the drain. The recombination models, activated in ATLAS via the key words CONSRH and AUGER, are essential for accurately capturing carrier recombination, which significantly influences capacity and charge transfer characteristics. Additionally, band gap narrowing is included to account for the properties of regions with high carrier concentration.

III.2 SOLUTION TECHNIQUE

SILVACO offers different methods for solving the semiconductor drift-diffusion (DD) equation alongside Poisson's equation across the mesh grid within the device structure. We adopt Newton's method to efficiently solve the Poisson's equation and electron continuity equations in the N-buried channel CCD. Poisson's equation, given by Equation (1) is solved for the electrostatic potential ψ

$$\nabla.(\varepsilon\nabla\psi) = -\mathrm{q}(\mathrm{p} - \mathrm{n} + N_D^+ - N_A^-) \quad (1)$$

Where ε is the permittivity, q is the electron charge, n and p are the electron and hole densities, and N_D^+ and N_A^- are the ionized donor and acceptor densities.The electron and hole continuity equations, represented by Equations (2, 3), are solved for the electron and hole concentrations:

$$\frac{\partial n}{\partial t} = \nabla.J_n + G_n - U_n \quad (2)$$

$$\frac{\partial p}{\partial t} = \nabla.J_p + G_p - U_p \quad (3)$$

Where J_n and J_p are the electron and hole current densities, and G_n and G_p are the generation rates.

The current density equations are given by Equations (4, 5):

$$J_n = q\mu_n nE + qD_n\nabla n \quad (4)$$

$$J_p = q\mu_p pE + qD_p\nabla p \quad (5)$$

Where μ_n and μ_n are the electron and hole mobilities, D_n and D_p are the diffusion coefficients, and E is the electric field.

IV. RESULTS

IV.1 ELECTRON CONCENTRATION DISTRIBUTION

The simulation begins by setting the drain bias to +14V, while maintaining all other gates at -6V. This initial step depletes

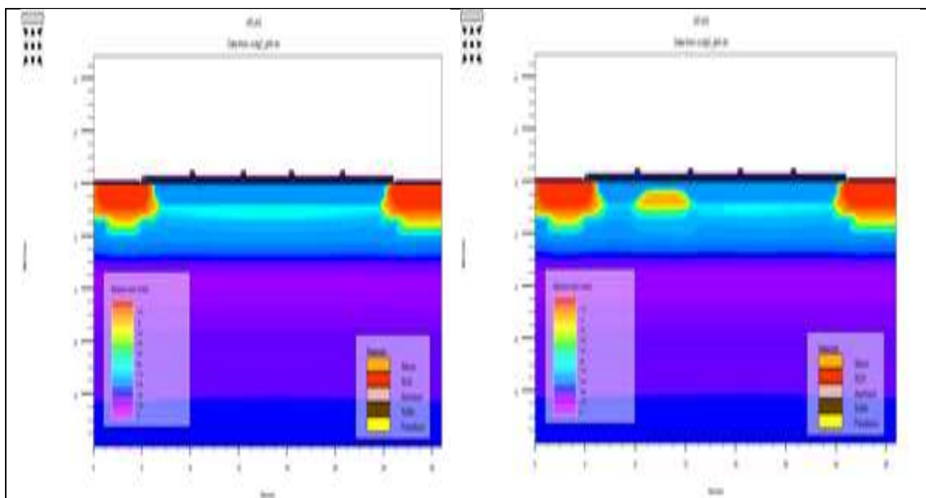

Figure 5: Surf of electron concentration distribution before and after signal charges.
Source: Authors, (2025).

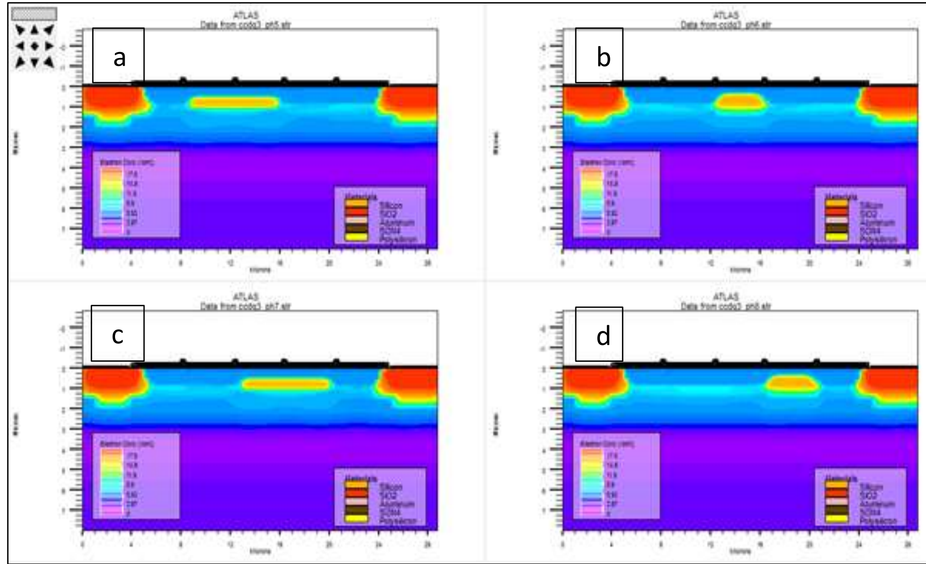

Figure 6: Surf of electron concentration distribution for signal charges transfer.
Source: Authors, (2025).

electrons from the n-type active layer. Following this, the storage gate is illuminated in a transient simulation, generating charge that is subsequently collected beneath the electrode gate G1. Figures 5 illustrate the electron concentration distribution before (left) and after (right) the formation of packet charges under gate G1. The electron concentration in the buried channel under non-illumination is observed to be at its minimum value (10^{10}cm^{-3}), indicating that no electrons are being generated or stored at this stage. After, illumination electrons charges are stored under gate G1 and peaks towards 10^{17}cm^{-3}, and the number of stored electrons reaches up to 1.5×10^{8}.

The gates within the device are interconnected in a periodic configuration to establish the CCD phases. The selected interconnection scheme as shown in Figure 2, determines the number of clocking voltages necessary to facilitate a unidirectional charge transfer towards the output drain. The transfer of packet charges under gates G2 and G3 is depicted in Figures 6(a, b, c, d).

IV.2 POTENTIAL AND ELECTRON CONCENTRATION PROFILES

A cross-section of potential and electron concentration along the y-line at $x = 0.6325\ \mu m$ is shown in Figure 7. This figure presents the electron concentration profile in the potential well, the electron density under gate G1, and the transfer process of electron density with corresponding potential profiles under gates 1 and 2.

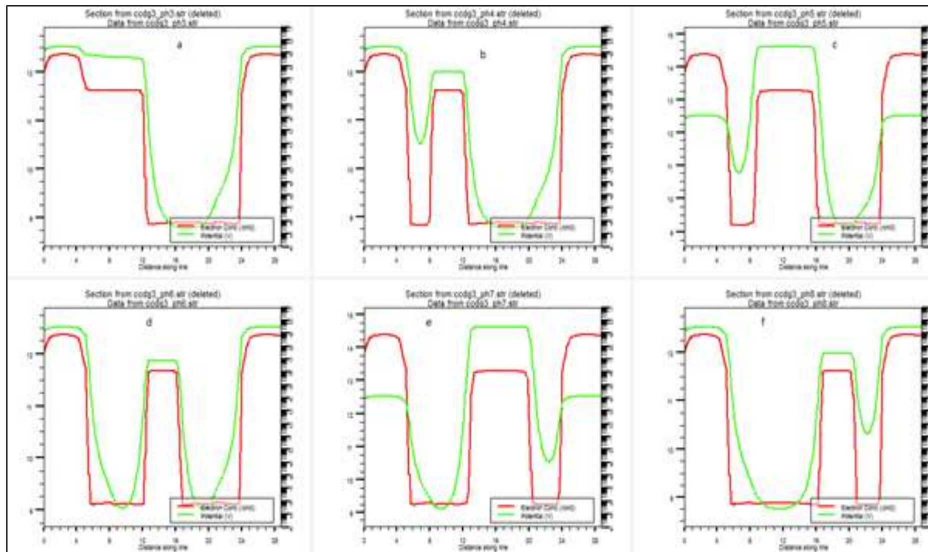

Figure 7: A cross section of potential and electron concentration along of ‘y’ line at $x = 0.6325\ \mu m$ (peak).
Source: Authors, (2025).

The trapped charge density resulting from the transfer of signal charge is evaluated once the signal packet has reached gate G3 is shown in Figure 6 (d) and Figure 7 (f). Due to emission, the trapped charge density decreases progressively from right to left. Since the charge spends significantly more time under the gates than in the gaps, the trapped charge density beneath the gates is considerably higher compared to the regions between them.

V. CHARGE TRANSFER INEFFICIENCY

Charge Transfer Inefficiency (CTI) measures the fractional loss of charge from a signal packet as it transfers across a pixel (three gates). The CTI for transfer over one gate is calculated using Equation (6) [14]:

$$CTI = \frac{Q_0 - Q_T}{Q_0} \quad (6)$$

Where Q_0 is the charge under the first gate, and Q_T is the charge transported to the second gate.

The CTI study incorporates bulk traps with energies 0.17 eV below the conduction band. These traps, created by incident particles with sufficient energy to displace atoms from their lattice points, introduce stable defects that manifest as energy levels [15,16]. The trap concentrations and electron capture cross-sections used in the simulations are 10^{11} cm^{-3} and 10^{-14} cm^{-2}, respectively. Following the simulation of the transfer process in ATLAS, a separate 2D integration of the trapped charge density distribution is carried out to determine the total charge beneath each gate.

V.1 CTI VERSUS TEMPERATURE

Figure 8 demonstrates the variation of CTI with temperature at a frequency of 4 MHz. The CTI peaks at 7x10^{-6} at 135 K, and optimal values are achieved around 200 K with a minimum CTI of 2x10^{-6}. This indicates that higher temperatures contribute to more efficient charge transfer, minimizing losses due to traps.

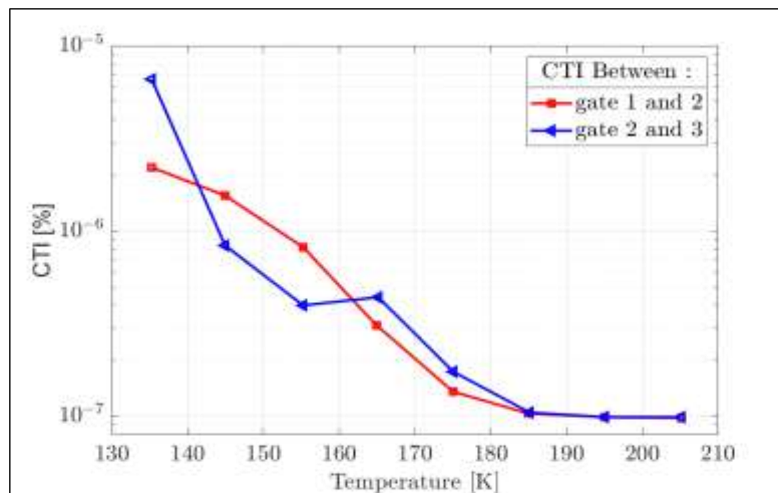

Figure 8: Charge transfer inefficiency against temperature at clocking frequency of 4 MHz.
Source: Authors, (2025).

It is observed that there is a general decrease CT with increasing temperature in the damaged device. Furthermore, the relationship between CTI and temperature exhibits a stronger nonlinear dependence [17].

VI. CONCLUSIONS

The Charge Transfer Inefficiency (CTI) in proton-damaged BCCD's is influenced by several parameters, particularly those associated with trap characteristics, including trap energy level, capture cross-section, and trap concentration (density). Additionally, operating conditions significantly impact CTI, as there is a strong temperature dependence on the trap emission rate, as well as a variation in CTI with the readout frequency. The buried charge-coupled device (BCCD) was comprehensively simulated using 2D process and simulation models implemented in the SILVACO software suite. This study analyzed the variation of CTI with temperature at a clock frequency of 4 MHz, incorporating partially filled traps at 0.17 eV below the conduction band. The results indicate that the optimal CTI values are achieved at temperatures around 200 K, with a minimum CTI of 2x10^{-6}, demonstrating the efficiency of charge transfer improves significantly at higher. The model predictions align well with the experimental results found in the literature. It is noted that there is a general decrease in CTI with increasing temperature in the damaged device. Additionally, the relationship between CTI and temperature demonstrates a pronounced nonlinear dependence. Finally, a significant advancement in enhancing the outcomes of this work would be to develop a 3D model, as the CTI is also influenced by the shape of the volume occupied by the signal packet.

VII. AUTHOR'S CONTRIBUTION

Conceptualization: Dahmane Djendaoui, Zoubir Becer and Thameur Obeidi.
Methodology: Dahmane Djendaoui, Zoubir Becer and Thameur Obeidi.
Investigation: Dahmane Djendaoui, Zoubir Becer and Thameur Obeidi.
Discussion of results: Dahmane Djendaoui, Zoubir Becer and Thameur Obeidi.
Writing – Original Draft: Dahmane Djendaoui.
Writing – Review and Editing: Dahmane Djendaoui, Zoubir Becer.
Resources: Dahmane Djendaoui, Zoubir Becer

Supervision: Dahmane Djendaoui, Zoubir Becer and Thameur Obeidi.
Approval of the final text: Dahmane Djendaoui, Zoubir Becer and Thameur Obeidi.

VIII. REFERENCES

[1] W. S. Boyle, G. E. Smith, "Charge coupled semiconductor devices", Bell Systems Technical Journal, vol. 49, no. 4, pp. 587–593, Apr. 1970.
DOI: 10.1002/j.1538-7305. 1970.tb01790.x

[2] M. lesser, "Charge-coupled device (CCD) image sensors", High Performance Silicon Imaging, Elsevier Ltd, pp. 75-93, **2020**.
https://doi.org/10.1016/B978-0-08-102434-8.00003-9

[3] I. Afanasieva. et al. "Astronomical Camera Based on a CCD261-84 Detector with Increased Sensitivity in the Near-Infrared", Photonics, vol. 10, no. 7, pp. 774, Jul. **2023**.
https://doi.org/10.3390/photonics10070774

[4] W, Zujun. et al., "Simulation for signal charge transfer of charge coupled devices", Journal of Semiconductors, vol. 30, no.12, 2009.
DOI 10.1088/1674-4926/30/12/124007

[5] B. Lu. et al. "Design and Characterizations of the Radiation-Hardened XCR4C ASIC for X-Ray CCDs for Space Astronomical Applications". IEEE Transactions on Nuclear Science, vol. 67, no. 6, pp. 1175 – 1184, June. **2020**. DOI: 10.1109/TNS.2020.2993402

[6] J. R. Janesick, "Scientific Charge-Coupled Devices". SPIE Press, 2001.
https://doi.org/10.1117/3.374903

[7] Silvaco Inc. Atlas user manual—Device Simulation Software, Silvaco Inc, Santa Clara, 2013.

[8] N. Bush, D. Hall, A. Holland, "Proton-induced traps in electron multiplying charge-coupled devices", Journal of Astronomical Telescopes, Instruments, and Systems, vol .7, no.1, Mar. **2021**
https://doi.org/10.1117/1.JATIS.7.1.016003

[9] O. Marcelot,, et al, "Study of CCD Transport on CMOS Imaging Technology: Comparison Between SCCD and BCCD, and Ramp Effect on the CTI", IEEE Transactions on Electron Devices, vol.61, no.3, pp. 844-849 Feb. 2014
DOI: 10.1109/TED.2014.2298693

[10] O. Marcelot, R. Molina, M. Bouhier and P. Magnan, "Design Impact on Charge Transfer Inefficiency of Surface CCD on CMOS Devices: TCAD and Characterization Study," in IEEE Transactions on Electron Devices, vol. 63, no. 3, pp. 1099-1104, March 2016,
Doi: 10.1109/TED.2016.2516045.

[11] S. Chahira, M. Mohammed, "Investigation of Space Radiation-Induced Effects on the Performance of CCD Detectors using Radiation Monitor's In-flight Measurements". IEEE Transactions on Nuclear Science, vol.72, no. 2, pp. 110 – 117, Dec. **2024**.
DOI**:** 10.1109/TNS.2024.3524761

[12] S. Parsons, et al, "Effects of temperature anneal cycling on a cryogenically proton irradiated CCD". *Journal of Instrumentation*, vol. *16, no.* 11, Nov. **2021**.
DOI: 10.1088/1748-0221/16/11/P11005

[13] H. C. Hsieh, T. W. Luk, "Two-dimensional transient analysis of a buried-channel charge-coupled device", Solid State Electronics, vol. 27, no. 3, pp.213-224, Mar. 1984.
https://doi.org/10.1016/0038-1101(84)90116-3

[14] A. Sopczak, "Modeling of charge transfer inefficiency in a CCD with high-speed column parallel readout", IEEE Transactions on Nuclear Science, vol. 56, no. 3, pp. 1613-1617, June. 2009.
DOI: 10.1109/TNS.2009.2020985

[15] W. Zujun, X. Yuanyuan, X. Rui, et al. "Charge transfer inefficiency increase of the CCD detector induced by proton and neutron irradiations". Nuclear Instruments and Methods in Physics Research Section A: Accelerators, Spectrometers, Detectors and Associated Equipment, vol. 978, Oct. **2020**.
https://doi.org/10.1016/j.nima.2020.164431

[16] S. André, A. Salim, B. Khaled, et al. "Radiation hardness studies in a CCD with high-speed column parallel readout". Journal of Instrumentation, vol. 3, no 05, May. 2008
DOI: 10.1088/1748-0221/3/05/P05007

[17] W. Lin, Z. Zitao, Z. Dong, et al. "Study on the mechanism of temperature effect on proton irradiated charge-coupled device", Radiation Effects and Defects in Solids, vol. 178, no 5-6, pp. 668-679. Jan. **2023**,
https://doi.org/10.1080/10420150.2023.2166837